P-Glycoprotein Function at the Blood–Brain Barrier Imaged Using ^{11}C-*N-Desmethyl*-Loperamide in Monkeys

Jeih-San Liow[1], William Kreisl[1], Sami S. Zoghbi[1], Neva Lazarova[1], Nicholas Seneca[1], Robert L. Gladding[1], Andrew Taku[1], Peter Herscovitch[2], Victor W. Pike[1], and Robert B. Innis[1]

[1]*Molecular Imaging Branch, National Institute of Mental Health, Bethesda, Maryland; and* [2]*PET Department, Clinical Center, National Institutes of Health, Bethesda, Maryland*

^{11}C-Loperamide is an avid substrate for P-glycoprotein (P-gp), but it is rapidly metabolized to ^{11}C-*N-desmethyl*-loperamide (^{11}C-dLop), which is also a substrate for P-gp and thereby contaminates the radioactive signal in the brain. Should further demethylation of ^{11}C-dLop occur, radiometabolites with low entry into the brain are generated. Therefore, we evaluated the ability of ^{11}C-dLop to quantify the function of P-gp at the blood–brain barrier in monkeys. **Methods:** Six monkeys underwent 12 PET scans of the brain, 5 at baseline and 7 after pharmacologic blockade of P-gp. A subset of monkeys also underwent PET scans with ^{15}O-water to measure cerebral blood flow. To determine whether P-gp blockade affected peripheral distribution of ^{11}C-dLop, we measured whole-body biodistribution in 4 monkeys at baseline and after P-gp blockade. **Results:** The concentration of ^{11}C-dLop in the brain was low under baseline conditions and increased 5-fold after P-gp blockade. This increase was primarily caused by an increased rate of entry into the brain rather than a decreased rate of removal from the brain. With P-gp blockade, uptake of radioactivity among brain regions correlated linearly with blood flow, suggesting a high single-pass extraction. After correction for cerebral blood flow, the uptake of ^{11}C-dLop was fairly uniform among brain regions, suggesting that the function of P-gp is fairly uniformly distributed in the brain. On whole-body imaging, P-gp blockade significantly affected distribution of radioactivity only to the brain and not to other visually identified source organs. The effective dose estimated for humans was approximately 9 μSv/MBq. **Conclusion:** PET with ^{11}C-dLop can quantify P-gp function at the blood–brain barrier in monkeys. The single-pass extraction of ^{11}C-dLop is high and requires correction for blood flow to accurately measure the function of this efflux transporter. The low uptake at baseline and markedly increased uptake after P-gp blockade suggest that ^{11}C-dLop will be useful to measure a wide range of P-gp functions at the blood–brain barrier in humans.

Received Jul. 23, 2008; revision accepted Sep. 3, 2008.
For correspondence or reprints contact: Jeih-San Liow, Molecular Imaging Branch, National Institute of Mental Health/National Institutes of Health, 31 Center Dr., Room B2B37, MSC 2035, Bethesda, MD 20892-2035.
E-mail: liowj@mail.nih.gov

Key Words: molecular imaging; radiotracer tissue kinetics; P-glycoprotein; loperamide; PET

J Nucl Med 2009; 50:108–115
DOI: 10.2967/jnumed.108.056226

The membrane-bound transporter P-glycoprotein (P-gp) acts as an efflux pump in several organs of the body (*1*). At the blood–brain barrier, P-gp and at least 3 other closely related transporters can block the entry of many drugs and toxins. These substrates have a wide variety of chemical structures but tend to be ampiphilic (i.e., have lipophilic components and a positive charge). The physiologic function of P-gp is thought to protect the brain from toxins in the blood. P-gp may also have pathophysiologic importance. For example, overexpression of P-gp may block the entry of anticonvulsant agents in the area of the epileptogenic focus (*2*). In addition, decreased P-gp function in Alzheimer disease (*3*) and Parkinson disease (*4*) may lead to the accumulation of amyloid or to the exposure of dopamine-containing neurons to exogenous toxins, respectively.

$^{99m/94m}$Tc-sestamibi (*5*) and ^{11}C-verapamil (*6*) are substrates of P-gp, but each of these agents has limitations for use at the blood–brain barrier. An effective radiotracer for P-gp at the blood–brain barrier should have high entry in the absence of P-gp. The function of P-gp can then be measured by the extent to which it blocks entry of the substrate radiotracer. In this regard, Tc-radiolabeled sestamibi is a poor agent for the brain, because the high molecular weight (783 atomic mass units) and positive charge of the radiotracer diminish its entry even in the absence of P-gp. Although ^{11}C-verapamil easily enters the brain after inhibition of P-gp, this radiotracer is rapidly metabolized to lipophilic radioactive compounds that also enter the brain. The presence of multiple radiolabeled species in the brain confounds quantitative analysis of P-gp function (*7*).

In the search for an improved radiotracer to measure P-gp function, we evaluated the ^{11}C-labeled version of

loperamide, a nonprescription medication used to treat diarrhea. Loperamide is an opiate agonist and acts on μ-receptors in the gut to slow motility and thereby treat diarrhea. Despite high doses and high plasma concentrations in human subjects, loperamide lacks central nervous system effects, because P-gp efficiently blocks virtually all brain entry (*8*). ^{11}C-loperamide is an avid substrate for P-gp at the blood–brain barrier. For example, brain uptake is increased several fold both in P-gp knock-out mice and in monkeys after pharmacologic blockade of P-gp (*9*). Unfortunately, ^{11}C-loperamide is rapidly metabolized to ^{11}C-*N-desmethyl*-loperamide (^{11}C-dLop), which is also an avid substrate for P-gp (*10*). Thus, after injection of ^{11}C-loperamide, brain radioactivity measured with PET derives from 2 compounds—namely, the parent radiotracer and its *N-desmethyl* metabolite. We compared ^{11}C-loperamide and ^{11}C-dLop in regard to the percentage contamination of brain radioactivity in P-gp knock-out mice at 30 min after injection of the radiotracer. For ^{11}C-loperamide, only 50% of extracted brain radioactivity was the parent radiotracer (*9*). In contrast, for ^{11}C-dLop, 90% of brain radioactivity was the parent radiotracer (*10*). Thus, compared with ^{11}C-loperamide, ^{11}C-dLop provides a PET signal from the brain of greater radiochemical purity, which allows the plasma concentrations of ^{11}C-dLop to be used as the sole input function for compartmental quantitation of P-gp function.

The primary purpose of this study was to evaluate the ability of ^{11}C-dLop to quantify P-gp function at the blood–brain barrier in monkeys. A secondary purpose of this study was to examine the distribution of radioactivity in the entire body at baseline and after P-gp blockade. Because P-gp is located in many organs, its blockade might alter the distribution and metabolism of ^{11}C-dLop and, thereby, indirectly affect uptake into the brain.

MATERIALS AND METHODS

Radiotracer Preparation

^{11}C-dLop was prepared by methylation of the primary amide precursor with ^{11}C-iodomethane (*10*). The radiotracer was prepared according to our Investigational New Drug Application 78260, submitted to the U.S. Food and Drug Administration (a copy of which is available at http://pdsp.med.unc.edu/snidd/). ^{11}C-dLop was obtained in high radiochemical purity (>99%) and with high specific activity at the time of injection (153.8 ± 111.1 GBq/μmol). The injected activity and specific activity of ^{11}C-dLop corresponded to a mass dose of 1.39 ± 0.76 μg (range, 0.33–2.38 μg).

PET Data Acquisition

Six male rhesus monkeys (11.9 ± 2.7 kg) underwent 12 PET scans of the brain; 5 scans were performed at baseline conditions and 7 were performed after P-gp blockade. Animals were immobilized with ketamine (10 mg/kg, intramuscularly), followed by anesthesia with 1.5% isoflurane in oxygen via an endotracheal tube. ^{11}C-dLop (320 ± 56 MBq in 10 mL) was injected intravenously, and PET scans were acquired for 90 or 120 min using a high-resolution research tomograph (Siemens Medical Solutions). Each scan consisted of 27 or 33 frames of increasing duration, from 30 s to 5 min. P-gp was blocked by ((2*R*)-anti-5-{3-[4-(10,11-dichloromethanodibenzo-suber-5-yl)piperazin-1-yl]-2-hydroxypropoxy}quinoline trihydrochloride (DCPQ) (8 or 16 mg/kg, intravenously), administered 30 min before ^{11}C-dLop. Eli Lilly provided DCPQ, which is a potent inhibitor of P-gp. DCPQ was previously reported as compound **14b** (*9*). Images were reconstructed using a list-mode ordered-subset expectation maximization algorithm. Scatter and attenuation correction were applied. All data were decay-corrected to the time of radiotracer injection.

Arterial Blood Sampling

In 5 of 6 monkeys, arterial blood was sampled from an indwelling catheter in the femoral artery. We obtained 18 blood samples in heparin-treated syringes during the 2-h scan. Plasma ^{11}C-dLop was quantified using radio–high-performance liquid chromatography (methanol:water:triethylamine [75:25:0.1, by volume] at 2.0 mL/min) and γ-counting. The plasma concentration of ^{11}C-dLop separated from radiolabeled metabolites was used as the input function for the compartmental analysis. The total concentration of radioactivity in whole blood was used for vascular correction of the PET data, assuming that blood constitutes 5% brain volume. Free fraction of ^{11}C-dLop in plasma was measured by ultrafiltration, as previously described (*11*).

Compartmental Analysis

MR images of each monkey were coregistered to the summed PET image of the entire scan. Eight brain regions were identified on the PET image with reference to the coregistered MR images. The regions and their volumes (cm^3) were frontal cortex (1.05 ± 0.14), anterior cingulate (0.31 ± 0.11), temporal cortex (0.72 ± 0.10), parietal cortex (1.16 ± 0.06), hippocampus (0.43 ± 0.11), occipital cortex (1.70 ± 0.19), putamen (0.78 ± 0.07), and cerebellum (1.10 ± 0.17). The concentration of radioactivity in each region was expressed as standardized uptake value (SUV): %SUV = (% injected activity per cm^3 brain) × (g body weight). One- and 2-tissue-compartment models were applied to calculate the rate constants (K_1, k_2, k_3, and k_4) and total distribution volume (V_T) (*12*). Nonlinear parameter fitting was performed using PMOD 2.9 (PMOD Technologies). The identifiability of the rate constants were obtained from the diagonal of the covariance matrix and expressed as a percentage of the variable itself.

Cerebral Blood Flow (CBF) Measurement

To measure CBF, 4 of the 6 monkeys received ^{15}O-water (^{15}O-H_2O) scans. For each monkey, 2 injections of ^{15}O-H_2O (148 MBq each) were administered, and each injection was followed by a 1-min acquisition. The water scans began at 30 min before each ^{11}C-dLop injection and were separated by 15 min to allow activity to decay. For the P-gp–blocked condition, the 2 water scans began at 15 min after the DCPQ injection. That is, DCPQ was given at 45 min before ^{11}C-dLop. In 2 of the 4 monkeys, we also measured radioactivity in continual arterial blood samples after injecting ^{15}O-H_2O. Regions of interest defined on the coregistered MR image for the ^{11}C-dLop image were applied directly to the water image, assuming no movement between the ^{15}O-H_2O and ^{11}C-dLop scans. Absolute blood flow was calculated using an autoradiographic method (*13*). With absolute blood flow (F) and K_1, we

further calculated the extraction fraction (E) using the following equation:

$$K_1 = F \cdot E, \quad \text{Eq. 1}$$

where

$$E = 1 - e^{(-PS/F)}, \quad \text{Eq. 2}$$

and PS is the permeability–surface-area product.

Whole-Body Dosimetry Study

Four male rhesus monkeys (12.1 ± 2.6 kg) underwent 7 whole-body PET scans at baseline and after P-gp blockade with DCPQ (8 mg/kg, intravenously). After an intravenous injection of ^{11}C-dLop (333 ± 60 MBq), 2-dimensional scans were acquired on the Advance tomograph (GE Healthcare) in 4 segments of the body (head to upper thigh) in frames of increasing duration (75 s to 15 min) for a total scan time of 120 min (22 frames). Tomographic images were compressed from front to back into a single planar image. Regions of interest were drawn over source organs that could be visually identified—namely, the brain, lungs, liver, kidneys, and thyroid. Residence times from the monkeys were converted into corresponding human values by a scaling factor based on organ and body weights of the 2 species, as described previously (*14*). Radiation absorption doses were calculated for a 70-kg adult male using OLINDA/EXM 1.0 (*15*).

RESULTS

P-gp Inhibition–Increased Brain Uptake

Under baseline conditions, the concentration of radioactivity in the brain was low (~50% SUV) and had low washout (Figs. 1A and 2A). To avoid overfitting the noise associated with low concentrations of radioactivity, we used only the 1-tissue model for compartmental analysis. The resulting values for V_T and K_1 were small in all brain regions, averaging 3.6 ± 0.6 mL·cm^{-3} and 0.035 ± 0.010 mL·cm^{-3}·min^{-1}, respectively (average of 8 brain regions from 3 scans in 3 monkeys).

After P-gp inhibition by DCPQ (8 mg/kg), radioactivity in the brain rapidly increased to a peak of 250% SUV (Figs. 1A and 2B). However, the washout was still slow, and radioactivity decreased only to 200% SUV at 120 min. The unconstrained 2-tissue-compartment model provided a better fit than did the 1-tissue-compartment model but with only marginal statistical significance (Fig. 1A; F test, $P < 0.05$). Furthermore, the 2-tissue-compartment model estimated the kinetic parameters, particularly k_3 and k_4, with poor identifiability (e.g., >50%). In contrast, the 1-tissue-compartment model estimated V_T, K_1, and k_2 with better identifiability (1%−5%). Therefore, we chose the 1-tissue-compartment model for subsequent analyses.

P-gp blockade increased V_T of ^{11}C-dLop by about 5-fold using the 1-tissue-compartment model. This increase was primarily due to an increase in K_1, because k_2 was similar at baseline and after P-gp blockade (Table 1). V_T of ^{11}C-dLop remained relatively stable over the 120 min of image acquisition (Fig. 3). For example, V_T calculated from 50 min of imaging was within 10% of that calculated from the entire 120 min.

Because radioactivity in the brain increased quickly and remained relatively stable after P-gp blockade, we evaluated the area under the time–activity curve as a simplified measure of brain uptake that does not require plasma measurements. This simplified analysis essentially assumes that brain uptake is irreversible and quantifies the accumulated uptake. Area under the time–activity curve from 0 to 30 min was linearly and strongly correlated with K_1 after P-gp blockade for the 8 brain regions in all 4 monkeys (Fig. 4A; all, $r > 0.95$).

The increased brain uptake of radioactivity caused by DCPQ was not a secondary, peripheral effect of increased concentration of ^{11}C-dLop in plasma. In fact, the peak concentration and clearance of ^{11}C-dLop from plasma were similar at baseline and after P-gp blockade (Fig. 1B). Furthermore, DCPQ had insignificant effects on the plasma-free fractions of ^{11}C-dLop, which were 15.4% ± 1.8% at baseline and 15.8% ± 1.4% after DCPQ in 3 monkeys ($P = 0.85$).

Effect of CBF

P-gp inhibition increased radioactivity to variable degrees in brain regions but always with the same rank order. For example, P-gp inhibition always increased radioactivity the most in the putamen and cerebellum and least in the

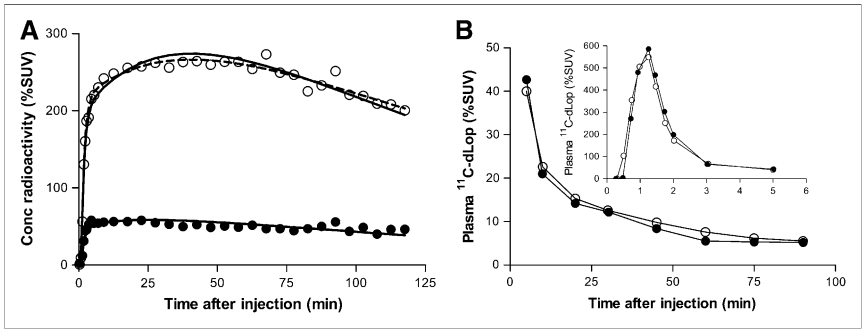

FIGURE 1. (A) Time–activity curve after injection of ^{11}C-dLop in temporal cortex fitted with 1-tissue-compartment (solid) and 2-tissue-compartment (dash) models at baseline (●) and after P-gp blockade (○) (DCPQ, 8 mg/kg, intravenously). Only 1-tissue-compartment model was used at baseline because of low brain uptake. All tissue curves were corrected for vascular volume, assuming that blood constitutes 5% brain volume. (B) Plasma parent radiotracer time–activity curve at baseline (●) and after P-gp blockade (○) in single monkey. Conc = concentration.

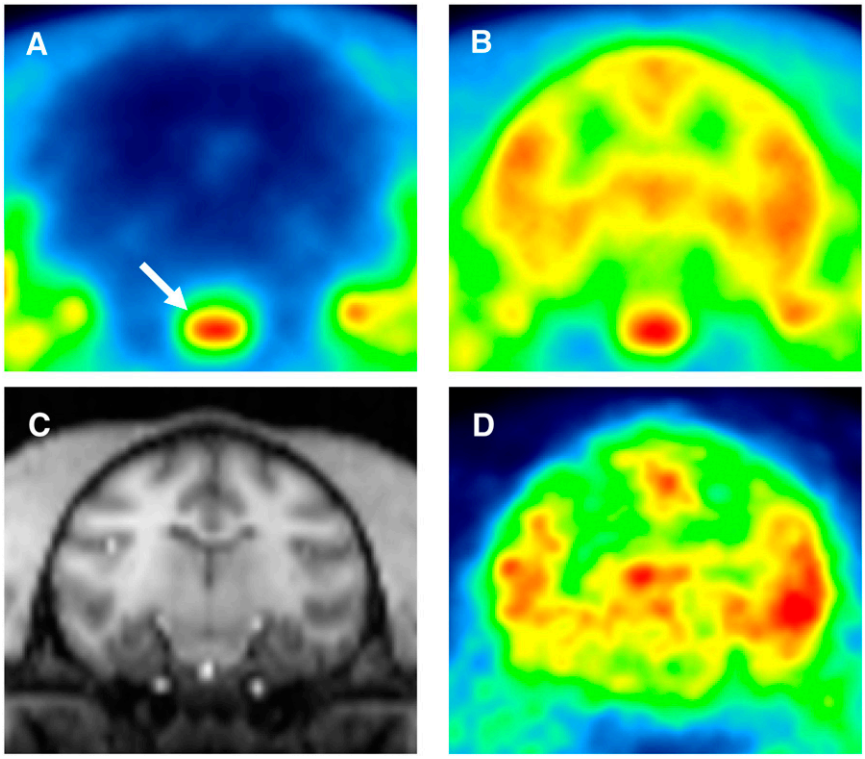

FIGURE 2. Total summed images (0–120 min) of ^{11}C-dLop at baseline (A) and after P-gp blockade (B). At baseline, all regions of brain except pituitary (A, arrow) had low uptake. (C) MR image coregistered with P-gp–blocked image of same monkey. (D) ^{15}O-H_2O scan of same monkey showing blood-flow pattern similar to that after injection of ^{11}C-dLop in B.

frontal cortex and hippocampus. We considered 2 possibilities for this differential uptake of ^{11}C-dLop. One possibility was that P-gp function is not uniformly distributed in the brain. A second possibility was that uptake is dependent on regional blood flow, which has reproducible patterns in anesthetized animals. For this second possibility, regions with higher blood flow would have greater uptake of radioactivity. In fact, ^{11}C-dLop uptake, measured using the area under the time–activity curve from 0 to 30 min, correlated linearly with relative blood flow in the 8 brain regions in all 4 monkeys. (Fig. 4B; $r = 0.94$, $P < 0.001$). The correlation was also observed visually by the similar distribution of radioactivity in the ^{11}C-dLop and ^{15}O-H_2O images (Figs. 2B and 2D).

We corrected brain uptake of ^{11}C-dLop for blood flow after P-gp blockade using a relative method, which compared flow in each region to that in the cerebellum. The scatter plot of blood flow versus ^{11}C-dLop uptake in the 8 regions was fitted to a straight line for each monkey (Fig. 5A). A linear correction was then applied to the time–activity curves (Fig. 5B) for ^{11}C-dLop in each region on the basis of blood flow relative to that in the cerebellum. As expected, this correction moved the regional curves together so they were almost overlapping for the initial 25–50 min (Fig. 5C). However, the curves began to diverge after about 50 min, suggesting that factors other than blood flow affect the latter portion of the time–activity curve. Nevertheless, these results show that, after correction for

TABLE 1. Rate Constants, V_T, and Goodness of Fit After P-gp Blockade, Using 1-Tissue-Compartment Model

Region	Rate constant		V_T (mL·cm^{-3})	Goodness of fit	
	K_1 (mL·cm^{-3}·min^{-1})	k_2 (min^{-1})		AIC	MSC
Frontal cortex	0.201 ± 0.031 (1.1 ± 0.2)	0.011 ± 0.004 (2.7 ± 0.7)	21.1 ± 8.3 (1.9 ± 0.6)	94 ± 9	4.1 ± 0.2
Anterior cingulate	0.251 ± 0.048 (1.7 ± 0.5)	0.011 ± 0.004 (3.9 ± 1.5)	24.2 ± 9.6 (2.8 ± 1.1)	121 ± 19	3.3 ± 0.5
Temporal cortex	0.25 ± 0.032 (1.1 ± 0.3)	0.011 ± 0.003 (2.6 ± 0.9)	24.2 ± 8.7 (1.9 ± 0.7)	96 ± 16	4 ± 0.4
Parietal cortex	0.229 ± 0.036 (1.1 ± 0.2)	0.011 ± 0.004 (2.4 ± 0.6)	22.6 ± 9.1 (1.7 ± 0.4)	93 ± 8	4.1 ± 0.1
Hippocampus	0.236 ± 0.057 (1.9 ± 0.2)	0.011 ± 0.003 (4.4 ± 1.0)	22.7 ± 9.3 (3.1 ± 0.9)	132 ± 7	2.8 ± 0.4
Occipital cortex	0.233 ± 0.035 (1.0 ± 0.2)	0.012 ± 0.005 (2.2 ± 0.7)	22.3 ± 9.4 (1.6 ± 0.6)	86 ± 13	4.4 ± 0.4
Putamen	0.331 ± 0.040 (1.0 ± 0.2)	0.011 ± 0.004 (2.2 ± 0.6)	31.7 ± 12.4 (1.6 ± 0.5)	87 ± 10	4.4 ± 0.2
Cerebellum	0.314 ± 0.051 (1.2 ± 0.4)	0.014 ± 0.004 (2.4 ± 0.9)	24.2 ± 9.3 (1.8 ± 0.7)	102 ± 23	3.9 ± 0.8

AIC = Akaike information criterion; MSC = model selection criterion.

P-gp was blocked by DCPQ (8 mg/kg, intravenously) administered 30 min before injection of ^{11}C-dLop. For each brain region, identifiability is listed in parentheses and is expressed as percentage of variable itself. Values are mean ± SD from 4 monkeys.

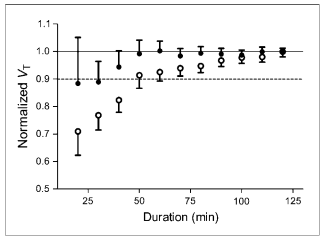

FIGURE 3. Time-stability curve of normalized V_T calculated with 1-tissue-compartment model for frontal cortex (○) and putamen (●), the 2 brain regions with lowest and highest uptake, respectively. Each curve was average from 4 monkeys after P-gp blockade (DCPQ, 8 mg/kg, intravenously). Error bars represent identifiability, expressed as percentage of variable itself. For each region, V_T was calculated with scan durations varying from 20 to 120 min, with 10-min increments. Value of V_T was normalized to that determined using entire 120 min.

relative blood flow, the uptake of ^{11}C-dLop was fairly uniform among these large brain regions, and therefore suggest that the function of P-gp is also fairly uniform in the brain.

Absolute Blood Flow and Extraction Fraction

Because the uptake of ^{11}C-dLop was dependent in part on blood flow, we measured absolute blood flow, which is required to calculate extraction fraction and permeability–surface-area product. Among these parameters, the primary effect of P-gp is on permeability (P). That is, P-gp decreases the permeability of drugs that are substrates for this efflux transporter. This primary effect to decrease permeability causes the values of E and K_1 to decrease (Eqs. 1 and 2).

In 3 of the 4 monkeys, absolute blood flow was calculated after injection of ^{15}O-H_2O by measuring radioactivity in arterial blood and the brain. Regional blood flow

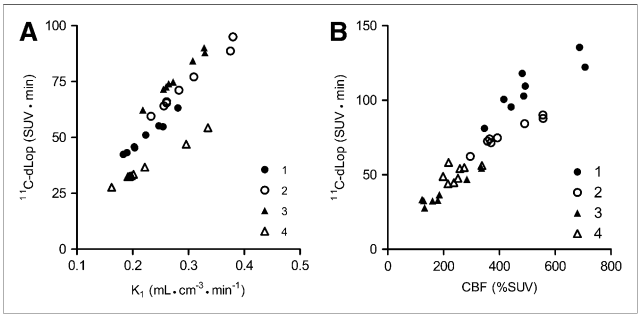

FIGURE 4. (A) Correlation between rate of brain entry (K_1) and area under time–activity curve of ^{11}C-dLop from 0 to 30 min after P-gp blockade. Area is expressed in units of concentration·time (SUV·min). Data represent 8 brain regions from 4 different monkeys. Correlation coefficients were greater than 0.99 for all 4 monkeys. (B) Correlation between relative CBF and area under time–activity curve of ^{11}C-dLop from 0 to 30 min after P-gp blockade. Data represent 8 brain regions from 4 different monkeys. CBF was measured as concentration of radioactivity (%SUV) in each brain region for 1 min after injection of 148 MBq of ^{15}O-H_2O.

(mL·cm^{-3}·min^{-1}) was similar at baseline (0.32–0.64) and after P-gp blockade (0.37–0.95; Table 2). Parietal cortex and putamen had the lowest and highest flow, respectively, under both conditions.

We estimated the single-pass extraction fraction (E) of ^{11}C-dLop by performing simulations using Equations 1 and 2. The simulated relationship between K_1 and F, based on a calculated mean extraction rate (from the 8 regions), fit the observed values for both baseline and P-gp blockade conditions (Fig. 6). The averaged extraction fraction of all 8 regions was 0.09 under the baseline condition but increased to between 0.31 and 0.58 after P-gp blockade (Table 2).

DCPQ could theoretically increase brain uptake by blocking P-gp or by increasing blood flow. To assess the latter possibility, we measured CBF at baseline and after P-gp blockade. Relative blood flow measured as %SUV did not show significant changes after DCPQ administration. In addition, absolute blood flow increased only 24% after DCPQ ($P < 0.01$; Table 2). In contrast, extraction increased about 5-fold. Thus, the primary effect of DCPQ to increase brain uptake of ^{11}C-dLop was inhibition of P-gp (as measured by increase in extraction) and not the relatively small increase in absolute blood flow.

Whole-Body Biodistribution

The brain, lungs, liver, and kidneys were visually identified as organs with moderate to high activities (Fig. 7). The liver had the highest uptake of ^{11}C-dLop, with an average peak of 39% injected activity at about 15 min after injection. The lungs and kidneys also exhibited relatively high uptake of radioactivity, with respective peak values of 31% and 11% injected activity at 2 min. Uptake in the brain slowly increased during the scan before leveling off at 2% injected activity at about 80 min. P-gp blockade had significant effects only in the brain, which increased from 2% at baseline to 3% injected activity after P-gp blockade.

Human residence times were estimated using average values from the planar images (Supplemental Table 1; supplemental materials are available online only at http://jnm.snmjournals.org). The organs with highest radiation exposure (μSv/MBq) were the thyroid (67), kidney (34), and liver (32) (Supplemental Table 2). P-gp blockade had significant effects only in the brain, for which radiation exposure increased from 3 to 5 μSv/MBq. The estimated effective dose (μSv/MBq) for humans was 9.4 and 8.9 at baseline and after P-gp blockade, respectively.

DISCUSSION

The purpose of this study was to evaluate the ability of ^{11}C-dLop to quantify P-gp function at the blood–brain barrier using compartmental modeling. P-gp blockade increased brain uptake of radioactivity about 5-fold, compared with low uptake at baseline (~50% SUV). As predicted from the mechanism of P-gp action, the increased

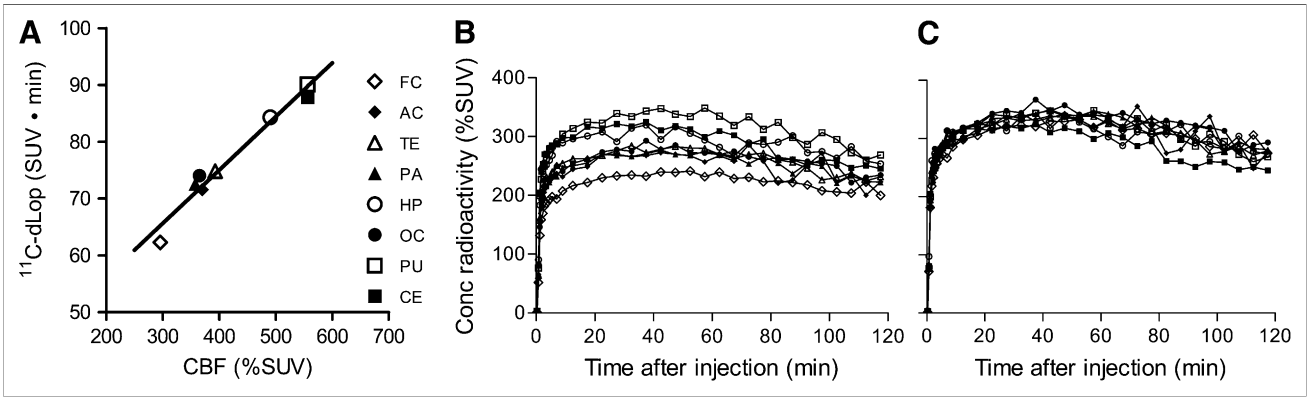

FIGURE 5. (A) Correlation of CBF and ^{11}C-dLop uptake for 8 brain regions in a single monkey after P-gp blockade. Time–activity curves of 8 regions before (B) and after (C) correction for blood flow based on fitted straight line in A. AC = anterior cingulate; CE = cerebellum; FC = frontal cortex; HP = hippocampus; OC = occipital cortex; PA = parietal cortex; PU = putamen; TE = temporal cortex.

uptake was primarily caused by an approximately 5-fold increase of entry into the brain (K_1), with minimal effect on exit from the brain (k_2). Our results are consistent with the finding that P-gp acts at the vascular endothelium (*16*) and prevents the entry of substrates into the brain. After P-gp blockade, brain uptake was rapid and dependent on blood flow. The effect of CBF was corrected with both relative and absolute measurements. With such corrections, brain uptake of ^{11}C-dLop in 8 relatively large regions was similar, which suggests that P-gp function is fairly uniformly distributed in the brain.

Whole-body imaging showed that the radiation exposure of ^{11}C-dLop is modest (~9 μSv/MBq), which is consistent with the short half-life of ^{11}C (20.4 min). Finally, P-gp blockade with DCPQ had relatively little effect on the distribution of radioactivity in the body, with the exception of the brain. This result confirmed that the effect of P-gp blockade to increase brain uptake was at the blood–brain barrier and not in the periphery.

Prolonged Retention of ^{11}C-dLop in Brain

After P-gp blockade with DCPQ, brain uptake of ^{11}C-dLop was rapid and relatively stable, despite rapidly declining concentrations of the radiotracer in plasma. We do not know the reasons for the prolonged retention of radioactivity in the brain, but it is unlikely to be due to either radiometabolites or receptor binding. Radiometabolites probably do not accumulate in monkey brains, because rodent studies showed that the vast majority (90%) of radioactivity extracted from the brain at 30 min was parent radiotracer (*10*). In addition, we previously reported that the brain uptake of ^{11}C-dLop could not be displaced by the opiate receptor antagonist naloxone or by loperamide itself (*10*). Thus, the prolonged uptake is not caused by reversible receptor binding. We do not know the reasons for the retention, but ionic trapping is a possibility. That is, intracellular ^{11}C-dLop may be protonated and trapped by a positive charge within a vesicle, as occurs with many drugs with a dissociation constant in the range of 7–8 (*17*).

TABLE 2. CBF and Extraction Fraction at Baseline and After P-gp Blockade

	CBF (mL·cm^{-3}·min^{-1})		Extraction fraction	
Region	Baseline	Blocked	Baseline (n = 3)	Blocked (n = 5)
Frontal cortex	0.37 ± 0.09	0.43 ± 0.17	0.09 ± 0.04	0.43 ± 0.10
Anterior cingulate	0.48 ± 0.12	0.54 ± 0.20	0.06 ± 0.03	0.42 ± 0.12
Temporal cortex	0.46 ± 0.07	0.58 ± 0.18	0.12 ± 0.03	0.4 ± 0.09
Parietal cortex	0.32 ± 0.02	0.37 ± 0.15	0.12 ± 0.06	0.57 ± 0.13
Hippocampus	0.43 ± 0.04	0.51 ± 0.15	0.12 ± 0.04	0.42 ± 0.13
Occipital cortex	0.31 ± 0.04	0.38 ± 0.19	0.12 ± 0.06	0.58 ± 0.10
Putamen	0.64 ± 0.07	0.95 ± 0.15	0.06 ± 0.02	0.31 ± 0.10
Cerebellum	0.61 ± 0.22	0.67 ± 0.12	0.05 ± 0.02	0.42 ± 0.13
Mean	0.45	0.56	0.09	0.44

P-gp was blocked by DCPQ, 8 mg/kg (n = 4) or 16 mg/kg (n = 1) intravenously, 30 min before injection of ^{11}C-dLop.
CBF is reported as mean ± SD from 3 monkeys. Extraction fraction was calculated using mean CBFs to left and averaged across monkeys.

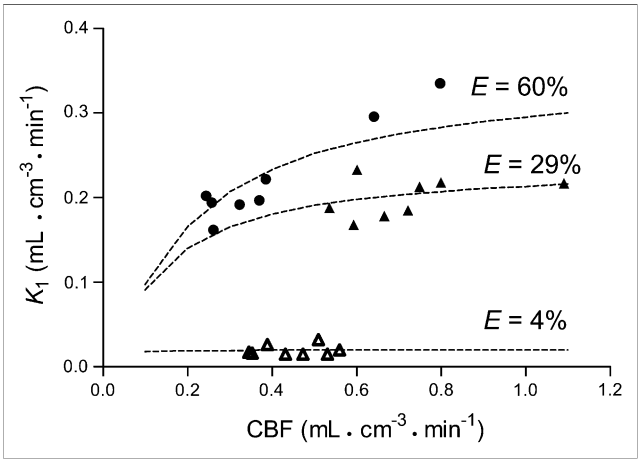

FIGURE 6. Correlation between absolute CBF and rate of brain entry (K_1) after injection of ^{11}C-dLop at baseline in 1 animal (△) and after P-gp blockade in 2 animals (● and ▲). Symbols represent 8 brain regions from each monkey. Curves show theoretic relationship between CBF and K_1 using Equations 1 and 2. Theoretic values of K_1 were generated using mean permeability and surface product (*PS*) calculated from CBF and K_1 of 8 regions for each study.

In fact, the apparent dissociation constant of dLop is 7.3 (*10*), which would allow ionic trapping in the acidic medium of vesicles such as lysosomes.

Extraction Fraction and Blood Flow

We calculated ^{11}C-dLop to have a single-pass extraction in the brain of about 40% (Table 2), meaning that about 40% of total ^{11}C-dLop in plasma entered the brain during each passage through the capillary bed. This extraction fraction is relatively large and is even larger than the plasma-free fraction of ^{11}C-dLop (~16%). Therefore, ^{11}C-dLop must dissociate from plasma proteins during the brief (1−2 s) passage through brain capillaries.

The extraction of ^{11}C-dLop after complete P-gp blockade is probably greater than 40%. We previously showed that DCPQ increased brain uptake of ^{11}C-dLop almost linearly in the dose range of 4–16 mg/kg (*10*), with no evidence of a maximal effect. Thus, complete P-gp blockade would increase brain uptake even further, implying that the extraction after complete blockade of P-gp would be greater than 40%.

The high brain extraction of ^{11}C-dLop and resulting dependence on blood flow have important implications for the capacity of P-gp and the measurement of its function. First, the high extraction (>40%) confirms both the rapidity and the high capacity of P-gp function at the blood–brain barrier. Our results in monkeys are consistent with prior studies in rats that showed the high capacity of P-gp at the blood–brain barrier, compared with the testes and lymphocytes (*18*). Second, because of the high extraction of ^{11}C-dLop, regional brain data should be corrected for blood flow to measure the function of P-gp.

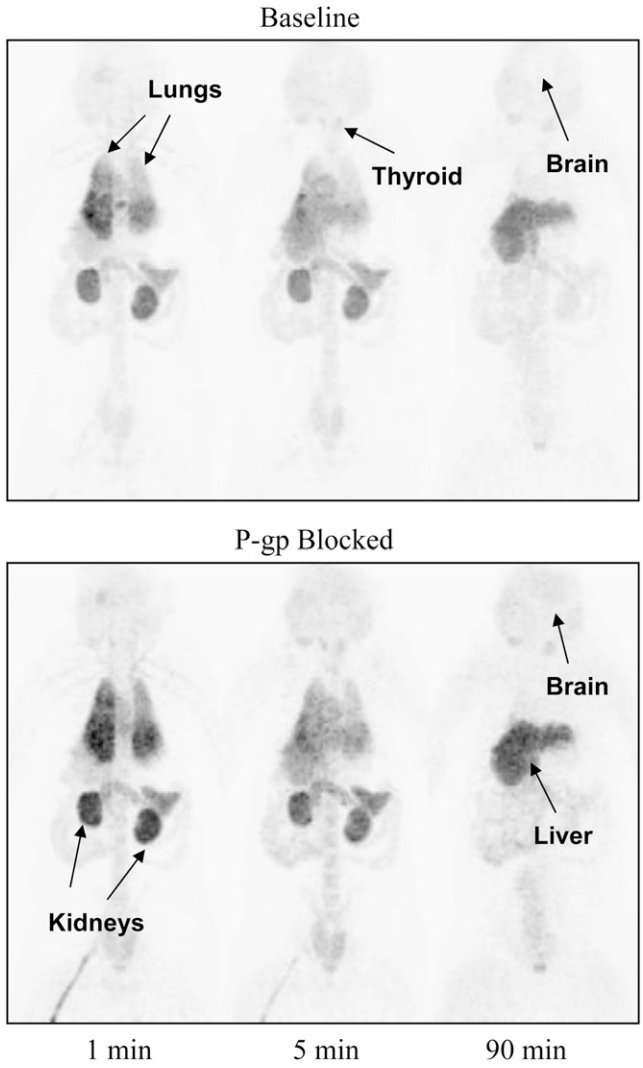

FIGURE 7. Maximum-intensity-projection images after injection of ^{11}C-dLop at baseline (top) and after P-gp blockade (bottom) conditions at 1, 5, and 90 min after radiotracer injection.

Whole-Body Dosimetry

In our whole-body biodistribution study of ^{11}C-dLop, we found the highest uptake of radioactivity in the liver, lungs, and kidneys. Despite the high uptake in the kidneys, little radioactivity was excreted via the urine (Fig. 7). Instead, the majority of radioactivity was likely excreted from the liver to the gastrointestinal tract. Should ^{11}C-dLop be demethylated (*10*), the resulting 1 carbon molecule could be exhaled as ^{11}C-carbon dioxide. We assessed this possibility by measuring the total radioactivity over the entire field of view (i.e., from head to mid thigh) over the 120 min of scanning. This measured radioactivity did not decline over time, suggesting that little radioactivity was exhaled during the course of the scan.

The distribution of radioactivity in organs of the body other than the brain is difficult to interpret relative to the known distribution of P-gp (*19*). For example, because P-gp

is known to excrete many drugs via the urine, we predicted the baseline scan would show significant accumulation of radioactivity in the urinary bladder and that P-gp blockade would decrease this route of excretion. In fact, under both baseline and blocked conditions, the kidney had high amounts of radioactivity, and the urinary bladder could not even be identified. The brain was the only organ that showed an easily interpreted effect. That is, P-gp blockade increased brain uptake from low levels at baseline to modest levels after P-gp blockade. The corresponding residence times increased from 0.013 h at baseline to 0.021 h after P-gp blockade. This modest 50% increase in radioactivity underestimated that from the kinetic brain studies, because the planar analysis used the compressed whole-body images. That is, the uptake at baseline (0.013 h) was artificially high, because the sampled region included muscle and skull anterior and posterior to the brain. In fact, the planar analysis may also explain why we saw no noticeable effect in peripheral organs, like the testes, known to express P-gp (i.e., tomographic imaging might have shown that P-gp blockade allowed entry of ^{11}C-dLop into some peripheral organs, such as the testes).

CONCLUSION

We found that ^{11}C-dLop is a promising radiotracer to measure P-gp function at the blood–brain barrier. Brain uptake is low at baseline, consistent with the rapid action and high capacity of P-gp. Pharmacologic blockade of P-gp causes about a 5-fold increase of peak brain activity, which is largely explained by about a 5-fold increase of brain entry (K_1). The single-pass extraction of ^{11}C-dLop is high ($>$40%) and requires correction for regional blood flow to determine the specific effects of P-gp to block entry of substrates into the brain.

ACKNOWLEDGMENTS

We thank Eli Lilly for providing DCPQ; Edward Tuan, Cheryl Morse, and Jinsoo Hong for their assistance in this study; the staff of the National Institutes of Health PET Department for successfully performing the PET studies; and PMOD Technologies (Zurich, Switzerland) for providing its image-analysis software. The Intramural Research Program of the National Institute of Mental Health supported this research (project Z01-MH-002795-07). A patent application has been filed on behalf of the U.S. government for PET imaging of P-gp function. Sami S. Zoghbi, Victor W. Pike, Neva Lazarova, and Robert B. Innis could personally benefit from this patent.

REFERENCES

1. Ambudkar SV, Dey S, Hrycyna CA, Ramachandra M, Pastan I, Gottesman MM. Biochemical, cellular, and pharmacological aspects of the multidrug tranporter. *Annu Rev Pharmacol Toxicol.* 1999;39:361–398.
2. Siddiqui A, Kerb R, Weale ME, et al. Association of multidrug resistance in epilepsy with a polymorphism in the drug-transporter gene ABCB1. *N Engl J Med.* 2003;348:1442–1448.
3. Cirrito JR, Deane R, Fagan AM, et al. P-glycoprotein deficiency at the blood-brain barrier increases amyloid-beta deposition in an Alzheimer disease mouse model. *J Clin Invest.* 2005;115:3285–3290.
4. Kortekaas R, Leenders KL, van Oostrom JC, et al. Blood-brain barrier dysfunction in parkinsonian midbrain in vivo. *Ann Neurol.* 2005;57:176–179.
5. Bigott HM, Prior JL, Piwnica-Worms DR, Welch MJ. Imaging multidrug resistance P-glycoprotein transport function using microPET with technetium-94m-sestamibi. *Mol Imaging.* 2005;4:30–39.
6. Takano A, Kusuhara H, Suhara T, et al. Evaluation of in vivo P-glycoprotein function at the blood-brain barrier among MDR1 gene polymorphisms by using ^{11}C-verapamil. *J Nucl Med.* 2006;47:1427–1433.
7. Lubberink M, Luurtsema G, van Berckel BN, et al. Evaluation of tracer kinetic models for quantification of P-glycoprotein function using (*R*)-[^{11}C]verapamil and PET. *J Cereb Blood Flow Metab.* 2007;27:424–433.
8. Sadeque AJ, Wandel C, He H, Shah S, Wood AJ. Increased drug delivery to the brain by P-glycoprotein inhibition. *Clin Pharmacol Ther.* 2000;68:231–237.
9. Zoghbi SS, Liow JS, Yasuno F, et al. ^{11}C-loperamide and its *N-desmethyl* radiometabolite are avid substrates for brain permeability-glycoprotein efflux. *J Nucl Med.* 2008;49:649–656.
10. Lazarova N, Zoghbi S, Hong J, et al. Synthesis and evaluation of [*N-methyl*-^{11}C]*N-Desmethyl*-loperamide as a new and improved PET radiotracer for imaging P-gp function. *J Med Chem.* 2008;51:6034–6043.
11. Gandelman MS, Baldwin RM, Zoghbi SS, Zea-Ponce Y, Innis RB. Evaluation of ultrafiltration for the free-fraction determination of single photon emission computed tomography (SPECT) radiotracers: beta-CIT, IBF, and iomazenil. *J Pharm Sci.* 1994;83:1014–1019.
12. Innis RB, Cunningham VJ, Delforge J, et al. Consensus nomenclature for in vivo imaging of reversibly binding radioligands. *J Cereb Blood Flow Metab.* 2007; 27:1533–1539.
13. Herscovitch P, Markham J, Raichle ME. Brain blood flow measured with intravenous $H_2{}^{15}O$. I. Theory and error analysis. *J Nucl Med.* 1983;24:782–789.
14. Seneca N, Cai L, Liow JS, et al. Brain and whole-body imaging in nonhuman primates with [^{11}C]MeS-IMPY, a candidate radioligand for beta-amyloid plaques. *Nucl Med Biol.* 2007;34:681–689.
15. Stabin MG, Sparks RB, Crowe E. OLINDA/EXM: the second-generation personal computer software for internal dose assessment in nuclear medicine. *J Nucl Med.* 2005;46:1023–1027.
16. Stewart PA, Beliveau R, Rogers KA. Cellular localization of P-glycoprotein in brain versus gonadal capillaries. *J Histochem Cytochem.* 1996;44:679–685.
17. al-Jaufy AY, King SR, Jackson MP. Purification and characterization of a Shiga toxin A subunit-CD4 fusion protein cytotoxic to human immunodeficiency virus-infected cells. *Infect Immun.* 1995;63:3073–3078.
18. Choo EF, Kurnik D, Muszkat M, et al. Differential in vivo sensitivity to inhibition of P-glycoprotein located in lymphocytes, testes, and the blood-brain barrier. *J Pharmacol Exp Ther.* 2006;317:1012–1018.
19. Fojo AT, Ueda K, Slamon DJ, Poplack DG, Gottesman MM, Pastan I. Expression of a multidrug-resistance gene in human tumors and tissues. *Proc Natl Acad Sci USA.* 1987;84:265–269.

Supplemental TABLE 1

Human residence times for ^{11}C-dLop extrapolated from rhesus monkeys

Source Organ	Residence time (h)					
	Baseline (n=4)			P-gp blocked (n=3)		
Brain	0.013	±	0.005	0.021	±	0.006
Thyroid	0.006	±	0.003	0.006	±	0.003
Lungs	0.096	±	0.046	0.075	±	0.037
Liver	0.187	±	0.102	0.164	±	0.056
Kidney	0.029	±	0.010	0.035	±	0.003
Remainder of Body	0.160	±	0.084	0.189	±	0.024

Data represents mean ± SD

Supplemental TABLE 2

Mean radiation dosimetry of ^{11}C-dLop extrapolated from the baseline scans of four monkeys.

Target Organ Doses	μSv/MBq	mrem/mCi
Adrenals	4.4 ± 0.5	16 ± 1.7
Brain	3.1 ± 1.3	12 ± 4.9
Breasts	1.8 ± 0.3	7 ± 1.0
Gallbladder Wall	5.6 ± 1.7	21 ± 6.1
LLI Wall	1.2 ± 0.5	5 ± 2.0
Small Intestine	1.9 ± 0.3	7 ± 1.3
Stomach Wall	2.3 ± 0.2	9 ± 0.7
ULI Wall	2.2 ± 0.3	8 ± 0.9
Heart Wall	3.2 ± 0.2	12 ± 0.8
Kidneys	34 ± 8.3	125 ± 31
Liver	32 ± 17	120 ± 62
Lungs	26 ± 11	95 ± 42
Muscle	1.7 ± 0.3	6 ± 1.2
Ovaries	1.4 ± 0.5	5 ± 1.9
Pancreas	3.7 ± 0.3	14 ± 1.1
Red Marrow	1.8 ± 0.2	7 ± 0.9
Osteogenic Cells	2.1 ± 0.6	8 ± 2.2
Skin	1.2 ± 0.3	4 ± 1.2
Spleen	2.4 ± 0.4	9 ± 1.6
Testes	1.0 ± 0.5	4 ± 1.8
Thymus	2.0 ± 0.4	8 ± 1.5
Thyroid	67 ± 34	247 ± 126
Urinary Bladder Wall	1.2 ± 0.5	4 ± 2.0
Uterus	1.4 ± 0.5	5 ± 1.9
Total Body	3.0 ± 0.1	11 ± 0.2
Effective Dose	**9.4 ± 1.1**	**35 ± 4.2**

Dosimetry estimates are based on a 70-kg human male

Data represents mean ± SD